Electrical Power and Energy Systems 157 (2024) 109792

Contents lists available at ScienceDirect

International Journal of Electrical Power and Energy Systems

journal homepage: www.elsevier.com/locate/ijepes

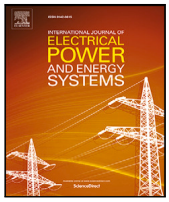

Frequency-dependent modeling of three-phase power cables for electromagnetic transient simulations

Caio G. Morata [a], Felipe Proença de Albuquerque [a], Pablo Torrez Caballero [b], Eduardo Coelho Marques da Costa [a,*], Ademir Pelizari [c]

[a] Department of Electronic Systems Engineering, Polytechnic School, University of São Paulo - POLI-USP, Brazil
[b] Federal University of Acre - UFAC, Rio Branco, Brazil
[c] Federal University of ABC - UFABC, Santo André, Brazil

ARTICLE INFO

Keywords:
Cable modeling
Electromagnetic transients
Offshore applications
Sector-shape cables
Power transmission

ABSTRACT

This paper proposes a methodology for modeling and simulating electromagnetic transients in power transmission cables with arbitrary cross-sections, usually applied in offshore power transmission and variable speed machine drive. This way, a sector-shaped cable is modeled taken into account its frequency-dependent parameters. Both impedance and admittance parameters are calculated by using the Finite Element Method, without analytic formulations based on the approach by an equivalent cylindrical cross-section, which leads to several inaccuracies. In sequence, the cable is decoupled into its four propagation modes by using an approximate modal transformation matrix with real and constant terms. Finally, each mode is modeled directly in the time domain by equivalent electric circuits, in which the lumped circuit elements are obtained from the rational function approach and fitting techniques.

1. Introduction

Renewable energy sources play an increasingly important role due to their low greenhouse gas emissions, low water consumption, and favorable social impacts. Transmission technologies effectively evolved together to accommodate renewable sources. Emerging transmission technologies such as submarine cables integrate offshore wind farms into shore-based electrical transmission and distribution systems [1–5].

For instance, power and telecommunication systems frequently use sector-shaped cables to interconnect offshore wind farms and low and medium-voltage distribution grids due to their smaller diameter than conventional coaxial and umbilical conductors with cylindrical cross-section [6].

Emerging cable technologies increase the electric power transmission capacity in both HVAC and HVDC systems. Non-conventional (non-cylindrical cross-section) conductor shapes reduce the cross-section area of power cables while increasing their transmission capacity. These configurations require more robust electrical insulation, alternative methods for parameter calculation, and modeling techniques for electromagnetic simulations [7–9].

Fig. 1 and Table 1 describe the geometric characteristics and electrical properties in the radial section of a typical sector-shaped cable, which is widely employed in submarine and underground power transmission systems, low and medium-voltage applications, and variable-speed machine driving [10,11].

Usually, the frequency-dependent parameter calculation by analytical methods, in the case of the sector-shaped cable, are based on the approximation of the arbitrary cross section by an equivalent cylindrical one, which leads to some errors and unrealistic results. Otherwise, methods based on the FEM — Finite Element Method proved to be more versatile, representing with great accuracy the geometric and structural characteristics of the cable, i.e. the proximity and skin effects in the conductors and parameters calculation [10,11].

The technical literature describes several analytic methods for electrical parameters calculation of cables composed of coaxial conductors with arbitrary cross sections. For example, a few methods have proposed the approach by an equivalent cylindrical transversal section, as prior presented [10,11]. Other methods proposed the representation of the arbitrary transversal section as being a set of elementary cylindrical conductors [6,12]. Nevertheless, such methods present some inaccuracies during parameter calculation at high frequencies, which leads to limitations in the modeling and simulation of electromagnetic transients composed of a wide range of frequencies. Finally, a few

* Corresponding author.
E-mail addresses: caio.morata@gmail.com (C.G. Morata), felipe.proenca.albuquerque@usp.br (F.P. de Albuquerque), pablotorrezcaballero@gmail.com (P.T. Caballero), educosta@usp.br (E.C.M. da Costa), ademir.pelizari@ufabc.edu.br (A. Pelizari).

https://doi.org/10.1016/j.ijepes.2024.109792
Received 4 August 2023; Received in revised form 12 December 2023; Accepted 9 January 2024
Available online 22 January 2024

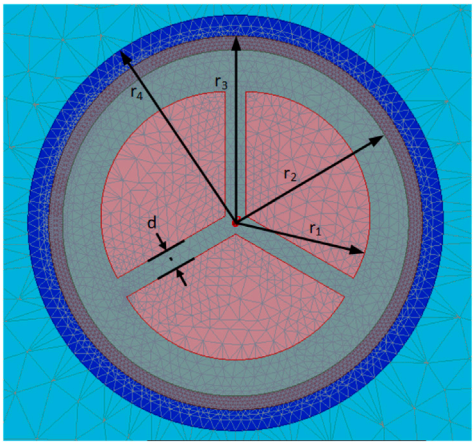

Fig. 1. Sector-shaped cable.

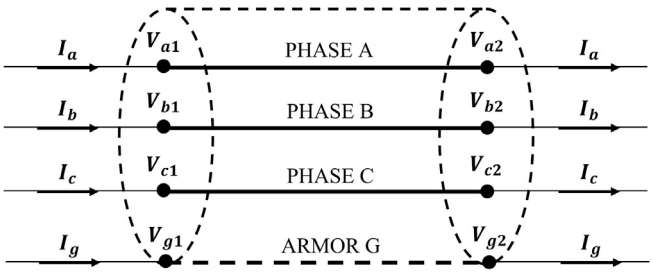

Fig. 2. Phase and armor conductors of the cable.

Table 1
Geometrical and physical characteristics of the sector-shaped cable.

Layer	Radius (mm)	σ (MS/m)	ϵ_r	μ_r
Cores	$r_1 = 19.00$	58.14	1.00	1.00
Inner insulation	$r_2 = 25.00$	0.00	4.10	1.00
Steel Armor	$r_3 = 27.00$	1.10	1.00	500
Outer insulation	$r_4 = 30.00$	0.00	2.30	1.00

methods have proposed a full-wave formulation to compute the modal electromagnetic fields and their corresponding modal currents and voltages [13]. These methods show great accuracy and complexity as well.

In this sense, a FEM-based method is proposed to calculate the frequency-dependent parameters, considering the sector-shaped cable's geometric and structural characteristics. The admittance and impedance parameters are determined from a frequency-varying input signal applied at the sending end of the cable, which induces a current density through the cross-section and an electric potential between conductors. The proposed method shows to be accurate for the entire range of frequencies considered in this research.

Since the frequency-dependent parameters of the sector-shaped cable are known, it can be modeled from the impedance fitting employing the rational function approach, equivalent circuit representation, and modal decoupling techniques [14,15]. However, a modal transformation matrix should be calculated, with real and constant terms, since the modeling by an equivalent circuit is determined directly in the time domain, and the three-phase approach, with Clarke's and Karrenbauer's matrices, cannot be applied to systems composed of more than three propagation modes. Thus, we propose an alternative algorithm to determine an approximated modal transformation matrix, composed of real and constant terms, for decoupling the phases and external armor of the cable into four independent modes. In sequence, each frequency-dependent mode can be modeled directly in the time domain, without numerical transforms, using the equivalent circuit representation and numerical solutions [16].

The proposed modeling methodology shows two main contributions. The first is the FEM-based method for calculation of the frequency-dependent parameters, without using the conventional analytical formulations and approach by an equivalent cylindrical conductor. The second goal is the simplified procedure in which the modal transformation matrix is determined, with real and constant terms, for modeling and simulation directly in the time domain.

2. Parameters calculation using a FEM-based algorithm

The computational platforms based on the Finite Element Method — FEM can simulate the electric potential between conductors, and current density through the radial section, in conventional cables as well as those characterized by arbitrary cross sections of the coaxial conductors.

The sector-shaped cable (Fig. 1) is composed of three coaxial conductors, with arbitrary geometry of the cross-section, and an external armor. The frequency-dependent electrical parameters are determined from simulations using a FEM-based computational platform, in which the current and voltage convention at the phases A, B, C, and external armor G are described in Fig. 2 at the sending and receiving ends of the cable (*port 1* and *port 2*, respectively).

The modeling and simulations are carried out with the multiphysics software ANSYS Maxwell 2D (FEM), following the cable descriptions in Fig. 1 and Table 1. Table 1 shows the radius of each layer of the sector-shaped cable, the electrical conductivity σ, the relative permittivity ϵ_r, and relative permeability μ_r. The distance between two phase conductors is $d = 4.25$ mm [10,17].

Note that the distance d in = 4.25 mm. Such a platform calculates the transversal capacitance between conductors, based on the electric potential and leakage current, which are determined from a frequency-varying voltage signal, applied at the sending end of the phase A, whereas the other phase conductors and external armor are grounded at this same terminal. Thus, the admittance matrix of the sector-shaped cable is determined from the nodal impedance matrix, according to the following expression

$$\begin{bmatrix} I_a - I_{a'} \\ I_b - I_{b'} \\ I_c - I_{c'} \\ I_g - I_{g'} \end{bmatrix} = \begin{bmatrix} Y_{aa} & Y_{ab} & Y_{ac} & Y_{ag} \\ Y_{ba} & Y_{bb} & Y_{bc} & Y_{bg} \\ Y_{ca} & Y_{cb} & Y_{cc} & Y_{cg} \\ Y_{ga} & Y_{gb} & Y_{gc} & Y_{gg} \end{bmatrix} \begin{bmatrix} V_a \\ V_b \\ V_c \\ V_g \end{bmatrix} \tag{1}$$

Terms I_a and $I_{a'}$ are the current at the sending end and shunt leakage current of phase A, since the receiving terminal of the cable is open during this simulation [10,17]. The same convention is applied to phase conductors B and C, and external armor G. The admittance terms are composed of imaginary parts only, *i.e.* admittance is then expressed in terms of a constant capacitance: $Y = j\omega C$. Transverse conductance is usually neglected in cable modeling, such as in overhead transmission line modeling [15].

Analogously, the frequency-dependent impedance parameters are calculated from the nodal admittance matrix. A frequency-varying current signal is applied at the sending end of the phase, whereas the other phases and armor are grounded at the same terminal. The three phases and armor are short-circuited at the receiving end. This way, the frequency-dependent resistance and inductance terms are calculated from the current density through the cross-section and voltage drop between sending and receiving ends of the cable, expressed as follows

$$\begin{bmatrix} V_{a1} - V_{a2} \\ V_{b1} - V_{b2} \\ V_{c1} - V_{c2} \\ V_{g1} - V_{g2} \end{bmatrix} = \begin{bmatrix} Z_{aa} & Z_{ab} & Z_{ac} & Z_{ag} \\ Z_{ba} & Z_{bb} & Z_{bc} & Z_{bg} \\ Z_{ca} & Z_{cb} & Z_{cc} & Z_{cg} \\ Z_{ga} & Z_{gb} & Z_{gc} & Z_{gg} \end{bmatrix} \begin{bmatrix} I_a \\ I_b \\ I_c \\ I_g \end{bmatrix} \tag{2}$$

Terms V_{a1} and V_{a1} are the voltage values at the sending and receiving ends of the phase conductor A. A similar convention is considered

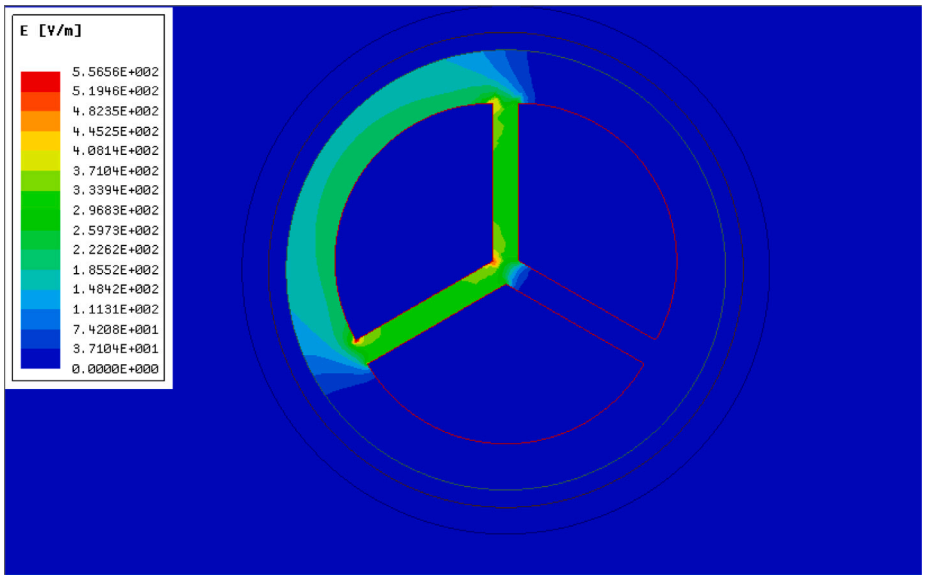

(a)

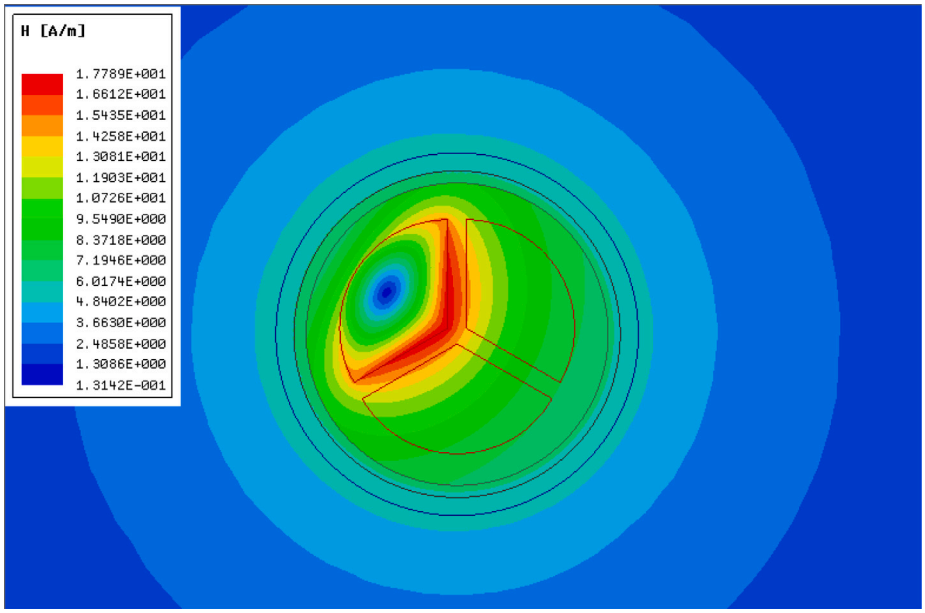

(b)

Fig. 3. Computed 3(a) Electric field and 3(b) magnetic field in the cable of Fig. 1.

for the phases B and C, and also for the armor G. The current terms at the receiving terminal, with the phase and armor sub-scripted, are I_a, I_b, I_c, and I_g. The current behavior in the cable is mainly determined as a function of the earth-return current and skin effect in the phase and armor conductors [10].

The electromagnetic simulations are performed from 10 Hz up to 1 MHz, which comprehends the vast majority of electromagnetic transients in power transmission systems [6,18].

For example, Figs. 3(a) and 3(b) describe the electric and magnetic fields impressed through the cross-section of the cable, from an input signal of 1 V and 60 Hz applied to the sending end of the phase A. Since the electric and magnetic field are calculated, the self and mutual capacitances and inductances can be also determined at 60 Hz. Analogously, the frequency-dependent parameters can be determined up to 1 MHz, by varying the frequency of the voltage input signal.

The FEM-based solver defines a variable mesh density on surfaces, where the electromagnetic phenomena are more pronounced. For example, the magnetic field is denser at the conductor boundaries of phase A, in which a frequency-varying signal was applied at the sending end, due to proximity and skin effects [9]. Thus, a higher mesh resolution in such domains is required, where the current density and magnetic field are more pronounced to improve the mapping accuracy. As expected, Figs. 3(a) shows that the electric field intensity is higher at the (sharp) corners of the conductors.

Since the required electromagnetic quantities are obtained, the frequency-dependent impedance parameters are calculated based on the Eq. (2). Figs. 4 and 5 show the resistance and inductance values.

Fig. 4 shows the self-resistance of the three phases, mutual resistances between two phases, and between phases and armor. The resistance terms of the impedance matrix $\boldsymbol{Z}$ can be determined by the analogy of the curves, due to the vertical symmetry of the transversal

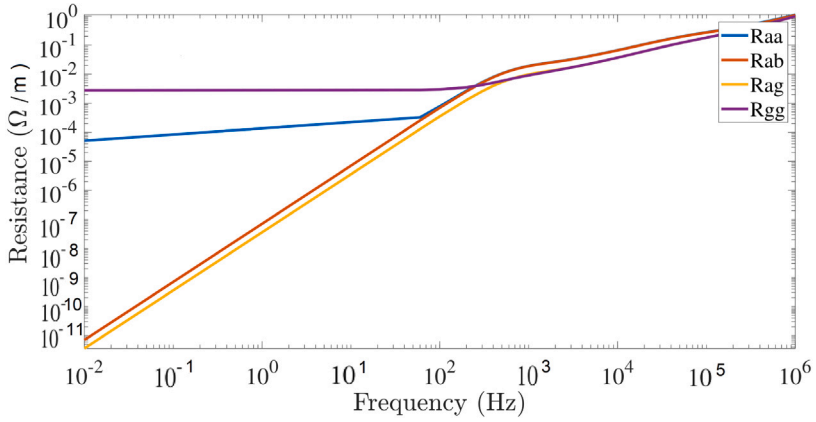

Fig. 4. Frequency-dependent resistance of the sector-shaped cable.

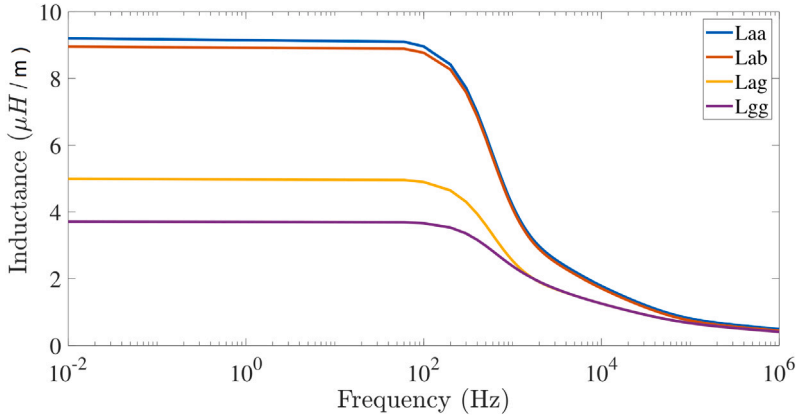

Fig. 5. Frequency-dependent inductance of the sector-shaped cable.

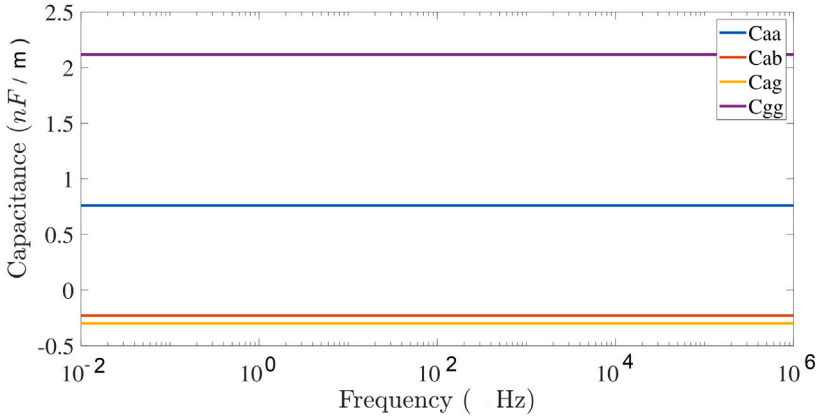

Fig. 6. Frequency-dependent capacitance of the sector-shaped cable.

section of the sector-shaped cable. Similarly, the frequency-dependent inductance values are determined, which represent the inductive reactance in the complex impedance (Fig. 5).

The admittance matrix is composed of frequency-dependent elements as well. However, the self and mutual capacitances are constant, such as described in the well-established literature on overhead transmission lines and cables [8,13]. Nevertheless, the capacitance values, obtained with the ANSYS Maxwell, are described in Fig. 6.

According to the technical literature, the capacitance terms in the admittance matrix $\boldsymbol{Y}$ are constant.

3. Multiconductor representation using modal decoupling

Modal decoupling has been widely used in the representation of multiconductor power systems. It decouples systems into independent propagation modes which can be represented as independent single-phase lines (propagation modes). The matrix of longitudinal

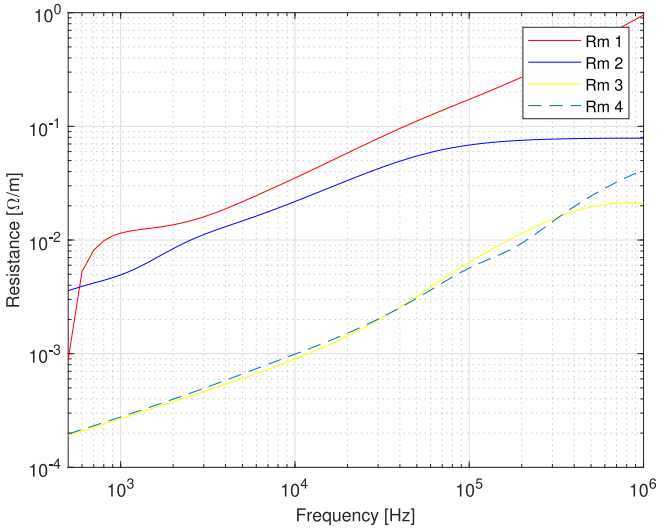

Fig. 7. Modal resistance R_m.

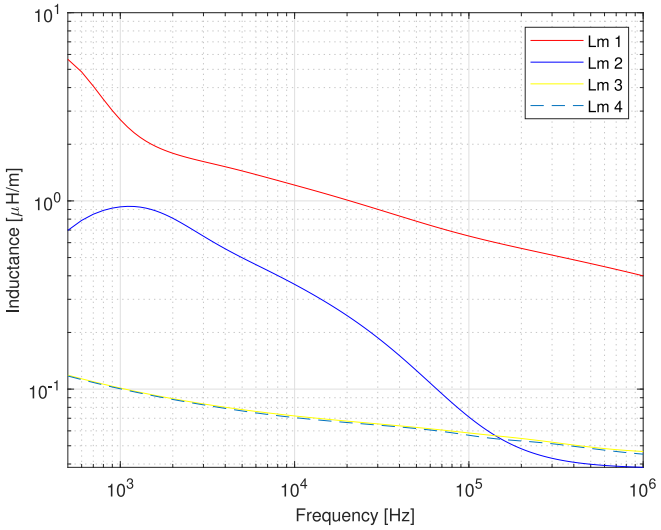

Fig. 8. Modal inductance L_m.

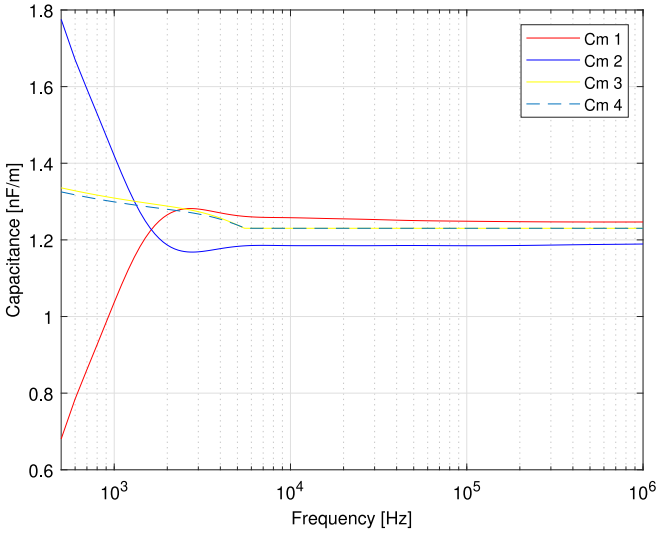

Fig. 9. Modal capacitance C_m.

impedances $\boldsymbol{Z}_{\mathrm{m}}$ and shunt admittances $\boldsymbol{Z}_{\mathrm{m}}$ of each mode is computed as follows [16]

$$\boldsymbol{Z}_{\mathrm{m}} = \boldsymbol{T}^{t}\boldsymbol{Z}\boldsymbol{T} \tag{3}$$

$$\boldsymbol{Y}_{\mathrm{m}} = \boldsymbol{T}^{-1}\boldsymbol{Y}\boldsymbol{T}^{-t} \tag{4}$$

where $\boldsymbol{Z}$ is the longitudinal impedance matrix, $\boldsymbol{Y}$ is the transversal admittance matrix, and $\boldsymbol{T}$ is the frequency-dependent modal transformation matrix, in which the columns are the eigenvectors of the product $\boldsymbol{Y}\boldsymbol{Z}$ [15]. The terms $\boldsymbol{T}^{-1}$ and $\boldsymbol{T}^{t}$ are the inverse and transposed forms of the modal transformation matrix $\boldsymbol{T}$, respectively.

The off-diagonal terms of $\boldsymbol{Z}$ and $\boldsymbol{Y}$ are implicitly representing the electromagnetic coupling between conductors. In this sense, the modal decoupling of systems with multiple phases, into independent propagation modes, shows to be a simplified solution for the explicit modeling of the mutual terms in $\boldsymbol{Z}$ and $\boldsymbol{Y}$, which represents a complex problem in the representation by equivalent electric circuits in the time domain [19,20].

The modal impedance matrix $\boldsymbol{Z}_{\mathrm{m}}$ and modal admittance matrix $\boldsymbol{Y}_{\mathrm{m}}$ are expressed as follows

$$\boldsymbol{Z}_{\mathrm{m}} = \begin{bmatrix} Z_1 & 0 & 0 & 0 \\ 0 & Z_2 & 0 & 0 \\ 0 & 0 & Z_3 & 0 \\ 0 & 0 & 0 & Z_4 \end{bmatrix} \tag{5}$$

$$\boldsymbol{Y}_{\mathrm{m}} = \begin{bmatrix} Y_1 & 0 & 0 & 0 \\ 0 & Y_2 & 0 & 0 \\ 0 & 0 & Y_3 & 0 \\ 0 & 0 & 0 & Y_4 \end{bmatrix} \tag{6}$$

The modal parameters $\boldsymbol{Z}_{\mathrm{m}}$ and $\boldsymbol{Y}_{\mathrm{m}}$, obtained from (5) and (6), are depicted in Figs. 7, 8, and 9. The cable is decoupled into four propagation modes, in which the p.u.l. resistance R_i, inductance L_i, and capacitance C_i are presented for modes 1, 2, 3, and 4. Values were computed based on a frequency range up to 1MHz, which is according to studies involving maneuvers and lightning impulses, such as suggested by the IEC and IEEE standards.

Both matrices in (5) and (6) have the off-diagonal terms null, which means that the four propagation modes are ideally decoupled. Thus, the current and voltage values of each mode are described as

$$\boldsymbol{I}_{\mathrm{m}} = \begin{bmatrix} I_1 & I_2 & I_3 & I_4 \end{bmatrix}^{t} \tag{7}$$

$$\boldsymbol{V}_{\mathrm{m}} = \begin{bmatrix} V_1 & V_2 & V_3 & V_4 \end{bmatrix}^{t}. \tag{8}$$

Since the modal decoupling was properly introduced for a generic cable with four propagation modes, the current and voltage transients can be simulated from two different approaches. First, each mode is represented by a two-port circuit in the frequency domain, in which the current and voltage are posteriorly determined in the time domain by using inverse transforms and convolutions [21]. The second approach is simulating the currents in $\boldsymbol{I}_{\mathrm{m}}$ and voltages in $\boldsymbol{V}_{\mathrm{m}}$ directly in the time domain, applying fitting techniques and equivalent circuit modeling [22,23].

Finally, the modal currents and voltages are converted to the phase domain, as described in (9) and (10).

$$\boldsymbol{I} = \boldsymbol{T}\boldsymbol{I}_{\mathrm{m}} \tag{9}$$

$$\boldsymbol{V} = \boldsymbol{T}^{-t}\boldsymbol{V}_{\mathrm{m}}. \tag{10}$$

Vectors $\boldsymbol{I}$ and $\boldsymbol{V}$ contain the currents and voltages of phase and armor.

Conventionally, the frequency-dependent matrix is applied to $\boldsymbol{Z}$ and $\boldsymbol{Y}$ decoupling them into $\boldsymbol{Z}_{\mathrm{m}}$ and $\boldsymbol{Y}_{\mathrm{m}}$, respectively, by using (3) and (4). However, in the proposed time-domain modeling with equivalent

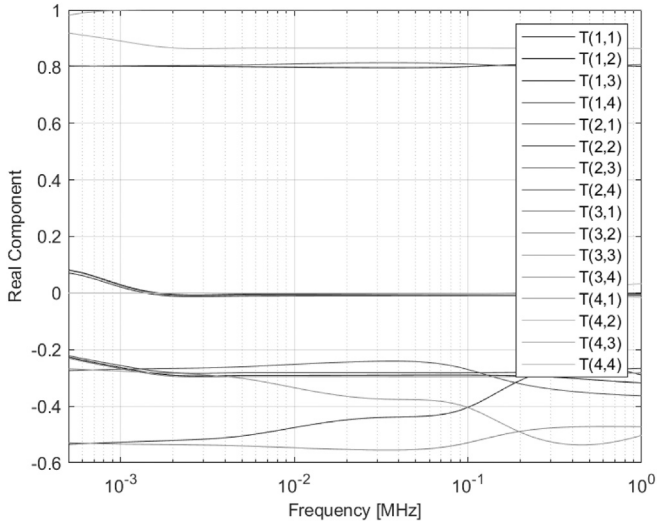

Fig. 10. Real part of the modal transformation matrix T.

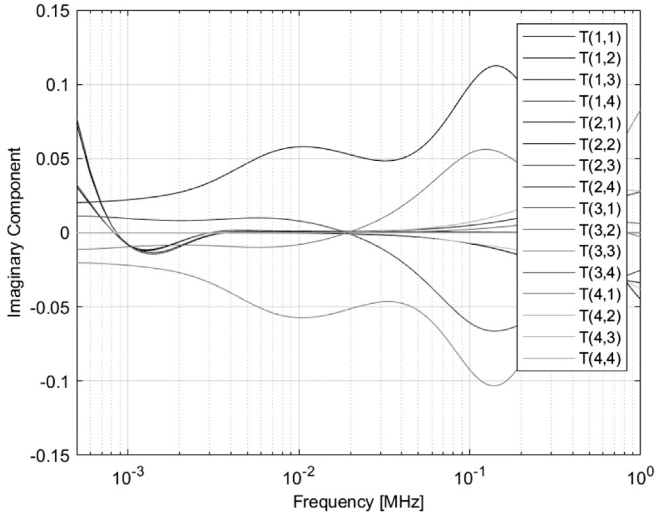

Fig. 11. Imaginary part of the modal transformation matrix T.

circuits, the same frequency-dependent matrix cannot be applied to convert $\boldsymbol{I}_{\mathrm{m}}$ and $\boldsymbol{V}_{\mathrm{m}}$ to the phase domain, from the phase-mode relationships in (9) and (10), because $\boldsymbol{I}$ and $\boldsymbol{V}$ are simulated directly in the time domain. Thus, the proposed methodology applies the frequency-dependent transformation matrix to decouple the cable parameters, in (3) and (4), and thereafter an approximated modal transformation matrix is used to convert the modal currents and voltages to the phase domain, mitigating eventual decoupling errors [24]. Nevertheless, the Clarke and Karrenbauer matrices cannot be applied to systems with more than four propagation modes. In this context, we propose an alternative and simplified procedure to determine a modal transformation matrix, composed of constant and real, from the parameters obtained with the FEM-based technique.

A real and constant transformation matrix, in (9) and (10), is obtained by sampling $\boldsymbol{T}$ at a given frequency f_{sampled} and discarding the remaining imaginary parts as follows

$$\boldsymbol{T}_{\mathrm{approx}} \approx \Re\{\boldsymbol{T}\left(f_{\mathrm{sampled}}\right)\} \tag{11}$$

Since the electromagnetic phenomenon to be analyzed is previously known, f_{sampled} can be estimated from the range of frequency in which the input signal is composed. Thus, the approximated matrix is set from a narrower interval than the entire range of frequencies, in which the electrical parameters were previously calculated (0,01 Hz–1 MHz). For example, f_{sampled} can be set up to 100 Hz for a maneuver or switching impulse because the electromagnetic transients produced from such input signal are mainly composed of frequencies up to 100 Hz. In this sense, the $\boldsymbol{T}_{\mathrm{approx}}$ is determined into a restricted frequency interval between 0.01 and 100 Hz, and no more into the entire frequency range up to 1 MHz, which mitigates eventual inaccuracies with the modal decoupling [24].

Figs. 10 and 11 show the real and imaginary parts of the modal transformation matrix $\boldsymbol{T}$ in (9) and (10). The real part of $\boldsymbol{T}$ varies up to 10 kHz, remaining relatively constant from 10 kHz to 1MHz. The imaginary parts of $\boldsymbol{T}$ are approximately null for the entire range of frequencies, as described in Fig. 11.

Based on the analysis of frequency-varying complex terms in $\boldsymbol{T}$, and an input signal composed of frequencies up to 10 kHz, an approximated modal transformation matrix can be determined for $f_{\mathrm{sampled}} = 1$ kHz, in which the terms are real and constant, without imaginary part.

In sequence, the setting of the approximated transformation matrix is evaluated based on results directly in the time domain, which is simulated using the proposed equivalent circuit in the time domain. The reference results for such analysis are determined from simulations using the two-port representation of the propagation modes, which are decoupled with the frequency-dependent transformation matrix $\boldsymbol{T}$. The two-port circuit is modeled in the frequency domain and the time-domain results are calculated by using numerical Laplace transforms [21].

4. Frequency-dependent modeling in the time domain

The sector-shaped cable of Fig. 1 is decoupled into its four modes. The frequency dependence of the longitudinal impedance of each mode is included in the time domain by combining fitting techniques and the PI circuit transmission line representation.

The conventional equivalent PI circuit does not consider the frequency effect on the longitudinal parameters of each propagation mode. In contrast, the frequency-dependent PI circuit fits the frequency-dependent longitudinal impedance of a propagation mode by means of a rational function, which is associated with an equivalent circuit in the longitudinal branch of each PI segment. The resulting frequency-dependent PI segment is cascaded to other frequency-dependent PI segments, in order to represent the distributed nature of the electrical parameters.

4.1. Frequency-dependent PI circuit

The longitudinal impedance of each mode is fitted to a rational function F_{fit} that is given by

$$F_{fit}(s) = d + se + \sum_{k=1}^{N_{real}} \frac{z_k}{s - p_k} + \sum_{k=1}^{N_{conj}} \left(\frac{z_k}{s - p_k} + \frac{z_k^*}{s - p_k^*} \right) \tag{12}$$

where d is the asymptotic high-frequency term, e is the linear term, N_{real} is the number of real poles, N_{conj} is the number of complex conjugate pairs of poles, z_k is the kth residue associated to the kth pole p_k, z_k^* is the kth conjugate residue associated to the kth conjugate pole p_k^*, and s is the complex frequency.

Fig. 12 shows the equivalent circuit that has an impedance $Z_{fit} = F_{fit}$ directly in the time domain using passive circuit elements.

The circuit of Fig. 12 consists of

- one series RL branch that represents the asymptotic high-frequency term d and linear term e;
- N_{real} parallel RL branches that represent real poles and their respective residues; and

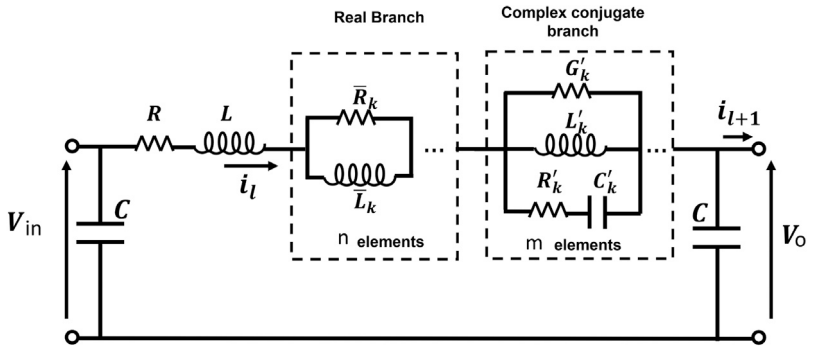

Fig. 12. Equivalent circuit.

- N_{conj} parallel RLGC branches that represent complex conjugate pairs of poles and their respective residues.

The circuit elements of the series RL branch are described as follows

$$R = d,\ L = e.$$

The circuit elements of the kth parallel RL branch are

$$R_k = z_k,\ L_k = -\frac{z_k}{p_k}.$$

Besides, the circuit elements of the kth complex conjugate branch are given by

$$L_k = \frac{-(z_k p_k^* + z_k^* p_k)}{p_k p_k^*}, \qquad G_k = \frac{1}{L_k}\left(\frac{z_k + z_k^*}{z_k p_k^* + z_k^* p_k} - \frac{p_k + p_k^*}{p_k p_k^*}\right),$$
$$R_k = \frac{z_k + z_k^*}{1 - G_k(z_k + z_k^*)}, \qquad C_k = -\frac{1}{R_k}\frac{z_k + z_k^*}{z_k p_k^* + z_k^* p_k}.$$

4.2. Representation by state equations

The Pi-circuit of Fig. 12 can be described by its state–space equations in which currents in inductors and voltages across capacitors are state variables $[\dot{X}_k]$, voltages at one terminal of the cable constitute the input variable, and voltages at the other terminal compose the output variable as follows

$$[\dot{X}_k] = [A_k][X_k] + [B_k][U_k] \tag{13}$$

In (13), vector $[X_k]$ has dimension $(n + 2m + 2) \times 1$, where n is the number of real branches and m is the number of complex branches in the circuit considered. $[A_k]$ matrix present in (13) is a square matrix with dimensions $(n + 2m + 2) \times (n + 2m + 2)$ and finally $[B_k]$ matrix has the same dimension of $[X_k]$ and this matrix is multiplied by the $[U_k]$ input voltage of the circuit.

The voltage across all inductors in the real branches is given by

$$\bar{L}_1 \frac{d}{dt} i_{\bar{1}} = \bar{R}_1 (i_l - i_{\bar{1}}) \tag{14}$$
$$\bar{L}_2 \frac{d}{dt} i_{\bar{2}} = \bar{R}_2 (i_l - i_{\bar{2}}) \tag{15}$$
$$\bar{L}_n \frac{d}{dt} i_{\bar{n}} = \bar{R}_n (i_l - i_{\bar{n}}). \tag{16}$$

The currents across inductors and capacitors in the complex branches are given by

$$L'_1 \frac{d}{dt} i'_{1_l} = \frac{1}{G'_1}(i_l - i'_{1_l} - i'_{1_c}) \tag{17}$$
$$L'_2 \frac{d}{dt} i'_{2_l} = \frac{1}{G'_2}(i_l - i'_{2_l} - i'_{2_c}) \tag{18}$$
$$L'_m \frac{d}{dt} i'_{m_l} = \frac{1}{G'_m}(i_l - i'_{m_l} - i'_{m_c}) \tag{19}$$
$$\frac{d}{dt} i'_{1_c} = \frac{C'_1}{(R'_1 C'_1 + 1)G'_1 + C'_1}\left(\frac{d}{dt} i_l - \frac{d}{dt} i'_{1_l}\right) \tag{20}$$
$$\frac{d}{dt} i'_{2_c} = \frac{C'_2}{(R'_2 C'_2 + 1)G'_2 + C'_2}\left(\frac{d}{dt} i_l - \frac{d}{dt} i'_{2_l}\right) \tag{21}$$
$$\frac{d}{dt} i'_{m_c} = \frac{C'_m}{(R'_m C'_m + 1)G'_m + C'_m}\left(\frac{d}{dt} i_l - \frac{d}{dt} i'_{m_l}\right). \tag{22}$$

Finally, the input current and output voltage of the equivalent circuit are given by

$$L_0 \frac{d}{dt} i_l = V_{i_n} - R_0 i_l - \bar{R}_1(i_l - i_{\bar{1}}) - \cdots - \bar{R}_n(i_l - i_{\bar{n}}) - \frac{1}{G'_1}(i_l - i'_{1_l} - i'_1 c) - \ldots - \frac{1}{G'_m}(i_l - i'_{m_l} - i'_{m_c}) - V_0 \tag{23}$$
$$\frac{d}{dt} V_0 = \frac{i_l}{C} - \frac{V_0}{C\ R_L} \tag{24}$$

Note that in (20)–(22), depends on V_{in} that is the input voltage of the PI circuit model associated with B_k matrix on (13). In (24), C and R_L are respectively the transversal capacitance and resistance load connected to the receptor terminal of the line. Note that the first capacitance from left to right in Fig. 12, is associated in parallel with the second to form C.

Using the provided equations, it is possible to derive the elements of (13). The complete expressions of the state–space equations are presented in Appendix A.1.

Then, with matrices X_k, A_k, and B_k, it is possible to model electromagnetic transient with one circuit of Fig. 12. In this paper, the vector fitting algorithm results in three real branches and one complex branch for the mode 1. For mode 2, four real branches and three complex branches are determined. The propagation mode 3 is represented by eight real branches and one complex branch, whereas mode 4 is represented by eight real branches.

After the frequency-dependent parameters fitting, each propagation mode is modeled as a single-phase line based on the equivalent circuit in Fig. 12, with the differential equations of the currents and voltages in the state space (13).

4.3. Cascade of frequency-dependent PI circuits

The cable approach by a cascade of frequency-dependent PI circuits can accurately represent the distributed nature of the electrical parameters. So, the frequency-dependent response is directly proportional to the number of equivalents PI circuits used in electromagnetic transient model [15].

Thus, the cascade PI circuits representation is a more accurately away to simulate a fast and impulsive electromagnetic transient than only one PI circuit. Because of cascade PI circuits is composed of a wide range of frequencies.

In Section 4.2, the state–space equation representation is made for a single PI circuit model representation. Now, this methodology will be expanded to h PI circuits in series connected like Fig. 13.

In Fig. 13, the $[X_k]$ vector is expanded to support all state variables for h PI circuits, utilized in series to model electromagnetic

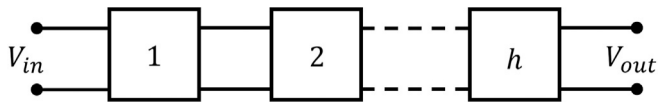

Fig. 13. Cascade of frequency-dependent PI circuit.

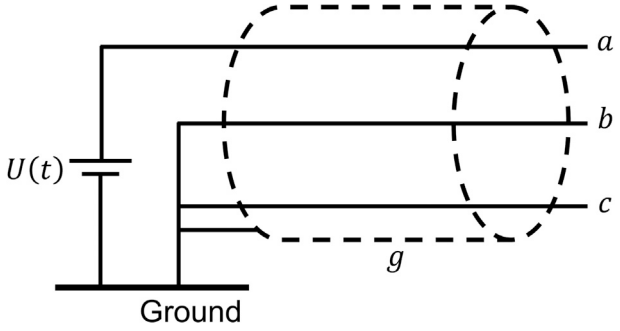

Fig. 14. Open Circuit test.

transient. To connect all PI circuits in series, is necessary to change some equations in state–space equation model.

Expanding the modeling to h PI circuits in cascade, the equation can be described in the following way.

$$\frac{d}{dt}\begin{bmatrix} \boldsymbol{x}_{series1} \\ \boldsymbol{x}_{series2} \\ \boldsymbol{x}_{series3} \\ \vdots \\ \boldsymbol{x}_{seriesh} \end{bmatrix} = \begin{bmatrix} \boldsymbol{A}_{series1} & \begin{bmatrix} \boldsymbol{A}_{11_2} & \boldsymbol{0} \end{bmatrix} & \boldsymbol{0} & \cdots & \boldsymbol{0} \\ \begin{bmatrix} \boldsymbol{0} & \boldsymbol{B}_k \end{bmatrix} & \boldsymbol{A}_{series2} & \begin{bmatrix} \boldsymbol{A}_{11_2} & \boldsymbol{0} \end{bmatrix} & \cdots & \boldsymbol{0} \\ \boldsymbol{0} & \begin{bmatrix} \boldsymbol{0} & \boldsymbol{B}_k \end{bmatrix} & \boldsymbol{A}_{series3} & \cdots & \boldsymbol{0} \\ \vdots & \vdots & \vdots & \vdots & \vdots \\ \boldsymbol{0} & \boldsymbol{0} & \boldsymbol{0} & \cdots & \boldsymbol{A}_{seriesh} \end{bmatrix} \begin{bmatrix} \boldsymbol{x}_{series1} \\ \boldsymbol{x}_{series2} \\ \boldsymbol{x}_{series3} \\ \vdots \\ \boldsymbol{x}_{seriesh} \end{bmatrix} + \begin{bmatrix} \boldsymbol{B}_k \\ \boldsymbol{0} \\ \boldsymbol{0} \\ \vdots \\ \boldsymbol{0} \end{bmatrix} \begin{bmatrix} \boldsymbol{U}_k \end{bmatrix} \tag{25}$$

The terms $A_{series1}$ until $A_{seriesh-1}$ present the relationship:

$$\begin{bmatrix} \boldsymbol{A}_{series1} \end{bmatrix} = \begin{bmatrix} \boldsymbol{A}_{11} & \boldsymbol{A}_{12} & \boldsymbol{A}_{1n+2} & \boldsymbol{A}_{1n+m+2} & \boldsymbol{A}_{1n+2m+2_2} \end{bmatrix}$$

While $A_{seriesh}$ has a little difference from others submatrices A_{series}, being represented in the following way

$$\begin{bmatrix} \boldsymbol{A}_{seriesh} \end{bmatrix} = \begin{bmatrix} \boldsymbol{A}_{11} & \boldsymbol{A}_{12} & \boldsymbol{A}_{1n+2} & \boldsymbol{A}_{1n+m+2} & \boldsymbol{A}_{1n+2m+2} \end{bmatrix}$$

The remaining elements are presented in Appendix A.2. Based on modeling technique described in this section, each propagation mode of the sector-shaped cable can be modeled as a cascade of PI circuits. The transient signals, like currents and voltages, are calculated for each propagation mode and can be converted to phase values using (9) and (10).

5. Time-domain simulations using the proposed model

Fig. 14 represents the sending end of the phase/core of the sector shaped-cable connected to a voltage source $U(t)$ and the other two phases and armor g connected at the sending end to the ground. All the phases and ground, are open at the receiving end. The sector-shaped cable, represented in Fig. 14, has 100 Km long and has the same characteristics and parameters calculated in Section 2.

The simulation consist of an unitary voltage step applied at the sending end of the phase a, represented in Fig. 14 by the voltage source $U(t)$. Results obtained from the proposed model, which each propagation mode is represented by 100 PI circuits in series (cascade), are simulated using the model transformation matrix in the frequency of 1 kHz.

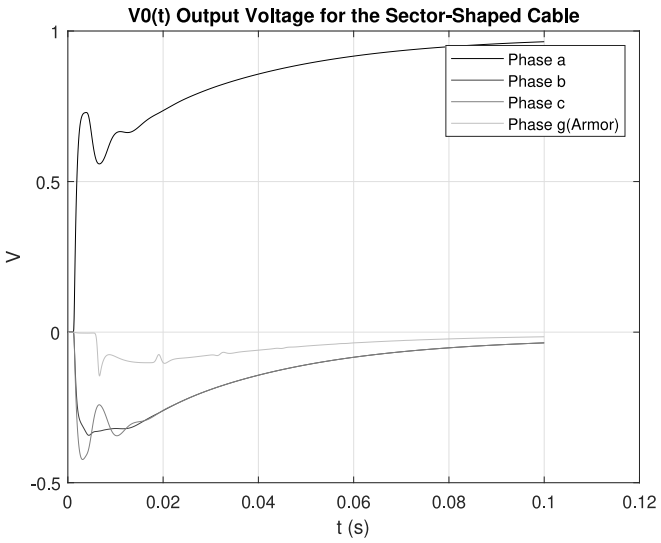

Fig. 15. Voltage transients at the receiving end of the phases a,b,c and armor g.

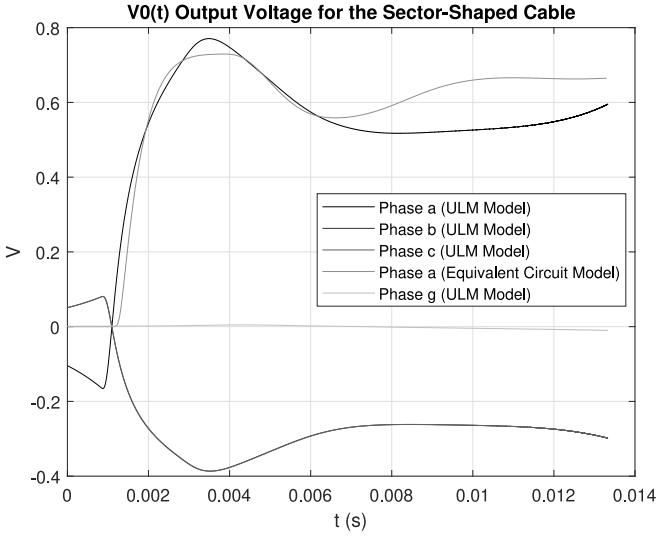

Fig. 16. Voltage transients at the receiving end of the phases a,b,c and armor g.

The voltages are explicitly represented in Fig. 15, for phases a, b, c and armor g. Fig. 15 shows that simulation obtained using the proposed model, fitting techniques for calculation of real and constant modal transformation matrix, and a frequency-dependent equivalent circuit of each propagation mode, represent the well known electromagnetic transient results for open circuit test with a switching impulse, represented by a unitary voltage step applied at the sending end of the phase a.

To better validate the proposed methodology, voltages are compared to the Numerical Laplace Transform (NLT), which model represents each mode as a two-port circuit in the frequency domain. Furthermore, the NLT proposed methodology consider the exact modal matrix $\boldsymbol{T}$, these two points are the differences between this model and the proposed model in this paper. Thus, the proposed modeling methodology can be validated comparing simulations obtained using the NLT, as reference results, and simulations carried out by the proposed model.

In Fig. 16, voltage of phase a is compared with the NLT results, where is possible to verify and validate the similarities between two different ways of modeling the sector-shaped cable.

6. Conclusions

This article presents a comprehensive approach to evaluate the parameters of a generic sector-shaped cable. The methodology incorporates a Finite Element Method modeling to calculate the inductance, resistance, and capacitance matrices, taking into account the presence of armor in the cable structure and the frequency effect on each element.

Furthermore, the coupled cable model is decomposed into propagation modes using modal transformation and a proposed approximation, aiming to simplify the calculation for a generic geometry.

The frequency-dependent parameters were represented using the Vector-Fitting approach, considering both real and imaginary branches, with their respective terms derived within the paper.

Finally, the time-domain model was developed in the state space with cascade of Pi-circuits, taken into account the frequency-dependent parameters. The simulations in the time domain show accuracy when compared to well-established models in the technical literature.

CRediT authorship contribution statement

Caio G. Morata: Data curation, Formal analysis, Investigation, Methodology, Software, Validation, Writing – original draft. **Felipe Proença de Albuquerque:** Methodology, Software, Supervision, Visualization, Writing – original draft. **Pablo Torrez Caballero:** Formal analysis, Methodology, Software, Supervision, Validation, Writing – review & editing. **Eduardo Coelho Marques da Costa:** Conceptualization, Formal analysis, Funding acquisition, Investigation, Methodology, Project administration, Resources, Supervision, Visualization, Writing – review & editing. **Ademir Pelizari:** Formal analysis, Investigation, Software, Supervision, Validation, Visualization.

Declaration of competing interest

The authors have no conflicts of interest to declare.

Data availability

No data was used for the research described in the article.

Acknowledgments

FAPESP - São Paulo Research Foundation (Grants 2021/01325-7 and 2019/05381-9).

CNPq - *Conselho Nacional de Desenvolvimento Científico e Tecnológico* (Grant 402830/2021-0).

TotalEnergies EP Brasil Ltda. and RCGI-USP (23.1.8493.1.9), sponsored by FAPESP (2020/15230-5).

ANP - Brazil National Oil, Natural Gas and Biofuels Agency through the R&DI levy regulation.

Appendix

A.1. State space equation for a single element

Consider the following description of the state space equation:

$$[\dot{X}_k] = [A_k][X_k] + [B_k][U_k]$$

The elements are described as:

$$\left[X_k\right] = \begin{bmatrix} i_l & i_{\bar{1}} & i_{\bar{2}} & \dots & i_{\bar{n}} & i'_{1_l} & i'_{2_l} & \dots & i'_{m_l} & i'_{1_c} & i'_{2_c} & \dots & i'_{m_c} & V_0 \end{bmatrix}^T$$

$$\left[\boldsymbol{A}_k\right] = \begin{bmatrix} \boldsymbol{A_{11}} & \boldsymbol{A_{12}} & \boldsymbol{A_{1n+2}} & \boldsymbol{A_{1n+m+2}} & \boldsymbol{A_{1n+2m+2}} \end{bmatrix}$$

where:

$$\left[\boldsymbol{A}_{11}\right] = \begin{bmatrix} \frac{\sum_{i=0}^{i=n} -R_{\bar{i}}}{L_0} & -\frac{1}{L_0 G'_1} & \dots & -\frac{1}{L_0 G'_m} \\ \frac{R_{\bar{1}}}{L_{\bar{1}}} & & & \\ \vdots & & & \\ \frac{R_{\bar{n}}}{L_{\bar{n}}} & & & \\ \frac{1}{L'_1 G'_1} & & & \\ \vdots & & & \\ \frac{1}{L'_m G'_m} & & & \\ \frac{-1}{R'_1 G'_1 + \frac{G'_1}{C'_1} + 1} \left(\frac{\sum_{i=0}^{i=n} R_{\bar{i}}}{L_0} + \frac{1}{L_0 G'_1} + \dots + \frac{1}{L_0 G'_m} + \frac{1}{L'_1 G'_1} \right) & & & \\ \vdots & & & \\ \frac{-1}{R'_m G'_m + \frac{G'_m}{C'_m} + 1} \left(\frac{\sum_{i=0}^{i=n} R_{\bar{i}}}{L_0} + \frac{1}{L_0 G'_1} + \dots + \frac{1}{L_0 G'_m} + \frac{1}{L'_m G'_m} \right) & & & \\ \frac{1}{C} & & & \end{bmatrix}$$

$$\left[\boldsymbol{A}_{12}\right] = \begin{bmatrix} \frac{R_{\bar{1}}}{L_{\bar{1}}} & \dots & \frac{R_{\bar{n}}}{L_0} \\ -\frac{R_{\bar{1}}}{L_{\bar{1}}} & \dots & 0 \\ \vdots & \vdots & \vdots \\ 0 & \dots & -\frac{R_{\bar{n}}}{L_{\bar{n}}} \\ 0 & \dots & 0 \\ \vdots & \vdots & \vdots \\ 0 & \dots & 0 \\ \frac{C'_1}{(R'_1 C'_1 + 1) G'_1 + C'_1} \left(\frac{R_{\bar{1}}}{L_0} \right) & \dots & \frac{C'_1}{(R'_1 C'_1 + 1) G'_1 + C'_1} \left(\frac{R_{\bar{n}}}{L_0} \right) \\ \vdots & \vdots & \vdots \\ \frac{C'_m}{(R'_m C'_m + 1) G'_m + C'_m} \left(\frac{R_{\bar{1}}}{L_0} \right) & \dots & \frac{C'_m}{(R'_m C'_m + 1) G'_m + C'_m} \left(\frac{R_{\bar{n}}}{L_0} \right) \\ 0 & \dots & 0 \end{bmatrix}$$

$$\left[\boldsymbol{A}_{1n+2}\right] = \begin{bmatrix} \frac{1}{L_0 G'_1} & \dots & \frac{1}{L_0 G'_m} \\ 0 & \dots & 0 \\ \vdots & \vdots & \vdots \\ 0 & \dots & 0 \\ -\frac{1}{L'_1 G'_1} & \dots & 0 \\ \vdots & \vdots & \vdots \\ 0 & \dots & -\frac{1}{L'_m G'_m} \\ \frac{C'_1}{(R'_1 C'_1 + 1) G'_1 + C'_1} \left(\frac{1}{L_0 G'_1} + \frac{1}{L'_1 G'_1} \right) & \dots & \frac{C'_1}{(R'_1 C'_1 + 1) G'_1 + C'_1} \left(\frac{1}{L_0 G'_m} \right) \\ \vdots & \vdots & \vdots \\ \frac{C'_m}{(R'_m C'_m + 1) G'_m + C'_m} \left(\frac{1}{L_0 G'_1} \right) & \dots & \frac{C'_m}{(R'_m C'_m + 1) G'_m + C'_m} \left(\frac{1}{L_0 G'_m} + \frac{1}{L'_m G'_m} \right) \\ 0 & \dots & 0 \end{bmatrix}$$

$$\left[\boldsymbol{A}_{1n+m+2}\right] = \begin{bmatrix} \frac{1}{L_0 G'_1} & \dots & \frac{1}{L_0 G'_m} \\ 0 & \dots & 0 \\ \vdots & \vdots & \vdots \\ 0 & \dots & 0 \\ -\frac{1}{L'_1 G'_1} & \dots & 0 \\ \vdots & \vdots & \vdots \\ 0 & \dots & -\frac{1}{L'_m G'_m} \\ \frac{C'_1}{(R'_1 C'_1 + 1) G'_1 + C'_1} \left(\frac{1}{L_0 G'_1} + \frac{1}{L'_1 G'_1} \right) & \dots & \frac{C'_1}{(R'_1 C'_1 + 1) G'_1 + C'_1} \left(\frac{1}{L_0 G'_m} \right) \\ \vdots & \vdots & \vdots \\ \frac{C'_m}{(R'_m C'_m + 1) G'_m + C'_m} \left(\frac{1}{L_0 G'_1} \right) & \dots & \frac{C'_m}{(R'_m C'_m + 1) G'_m + C'_m} \left(\frac{1}{L_0 G'_m} + \frac{1}{L'_m G'_m} \right) \\ 0 & \dots & 0 \end{bmatrix}$$

$$\left[\boldsymbol{A}_{1n+2m+2}\right]=\begin{bmatrix} -\frac{1}{L_0} \\ 0 \\ \vdots \\ 0 \\ 0 \\ \vdots \\ 0 \\ -\frac{C'_1}{(R'_1C'_1+1)G'_1+C'_1}\frac{1}{L_0} \\ \vdots \\ -\frac{C'_m}{(R'_mC'_m+1)G'_m+C'_m}\frac{1}{L_0} \\ -\frac{1}{CR_L} \end{bmatrix},\quad \left[B_k\right]=\begin{bmatrix} \frac{1}{L_0} \\ 0 \\ 0 \\ \vdots \\ 0 \\ \frac{C'_1}{(R'_1C'_1+1)G'_1+C'_1}\frac{1}{L_0} \\ \frac{C'_2}{(R'_2C'_2+1)G'_2+C'_2}\frac{1}{L_0} \\ \vdots \\ \frac{C'_m}{(R'_mC'_m+1)G'_m+C'_m}\frac{1}{L_0} \\ 0 \end{bmatrix}$$

A.2. Description of the state space equation for the cascade pi-model

The remaining elements of the cascade Pi-model are described as follows:

$$\left[\boldsymbol{A}_{1n+2m+2_2}\right]=\begin{bmatrix} -\frac{1}{L_0} \\ 0 \\ \vdots \\ 0 \\ 0 \\ \vdots \\ 0 \\ -\frac{C'_1}{(R'_1C'_1+1)G'_1+C'_1}\frac{1}{L_0} \\ \vdots \\ -\frac{C'_m}{(R'_mC'_m+1)G'_m+C'_m}\frac{1}{L_0} \\ 0 \end{bmatrix}\left[\boldsymbol{A}_{11_2}\right]=\begin{bmatrix} 0 \\ 0 \\ \vdots \\ 0 \\ 0 \\ \vdots \\ 0 \\ 0 \\ \vdots \\ 0 \\ -\frac{1}{C_s} \end{bmatrix}$$

References

[1] Gouda OE, Dein AZE. Improving underground power distribution capacity using artificial backfill materials. IET Gener Transm Distrib 2015;9:2180–7. http://dx.doi.org/10.1049/iet-gtd.2015.0274.

[2] Lazaropoulos AG. Numerical evaluation of broadband transmission characteristics of underground low-voltage networks - introducing techno-pedagogical (TP) method. Int J Electr Power Energy Syst 2014;55:253–60. http://dx.doi.org/10.1016/j.ijepes.2013.09.009.

[3] Marshall JS, Hines PD, Zhang JD, Minervini F, Rinjitham S. Modeling the impact of electric vehicle charging on heat transfer around underground cables. Electr Power Syst Res 2013;97:76–83. http://dx.doi.org/10.1016/j.epsr.2012.12.006.

[4] Kabalci E, Kabalci Y, Develi I. Modelling and analysis of a power line communication system with qpsk modem for renewable smart grids. Int J Electr Power Energy Syst 2012;34:19–28. http://dx.doi.org/10.1016/j.ijepes.2011.08.021.

[5] Papadopoulos TA, Chrysochos AI, Papagiannis GK. Analytical study of the frequency-dependent earth conduction effects on underground power cables. IET Gener Distrib Transm 2013;7:276–87. http://dx.doi.org/10.1049/iet-gtd.2012.0425.

[6] Kariyawasam KKMA, Gole AM, Kordi B, De Silva HMJSP. Accurate electromagnetic transient modeling of sector-shaped cables. In: International conference on power systems transients. 2011, p. 1–6.

[7] Brito AI, Machado VM, Almeida ME, Neves MG. Skin and proximity effects in the series-impedance of three-phase underground cables. Electr Power Syst Res 2016;130:132–8. http://dx.doi.org/10.1016/j.epsr.2015.08.027.

[8] Bonyadi-ram S, Kordi B, Bridges GE. A full-space conformal mapping for the calculation of series impedance of overhead transmission lines and underground cables. Electr Power Syst Res 2012;91:95–103. http://dx.doi.org/10.1016/j.epsr.2012.05.005.

[9] Gudmundsdottir US. Proximity effect in fast transient simulations of an underground transmission cable. Electr Power Syst Res 2014;115:50–6. http://dx.doi.org/10.1016/j.epsr.2014.03.016.

[10] Ametani A. A general formulation of impedance and admittance of cables. IEEE Trans Power Appar Syst 1980;PAS-99(3):902–10. http://dx.doi.org/10.1109/tpas.1980.319718.

[11] Ametani A, Fuse I. Approximate method for calculating the impedances of multiconductors with cross sections of arbitrary shapes. Electr Eng Japan 1992;112(2):117–23. http://dx.doi.org/10.1002/eej.4391120213.

[12] Lucas R, Talukdar S. Advances in finite element techniques for calculating cable resistances and inductances. IEEE Trans Power Appar Syst 1978;PAS-97(3):875–83. http://dx.doi.org/10.1109/tpas.1978.354559.

[13] Habib S, Kordi B. Calculation of multiconductor underground cables high-frequency per-unit-length parameters using electromagnetic modal analysis. IEEE Trans Power Deliv 2013;28(1):276–84. http://dx.doi.org/10.1109/tpwrd.2012.2224382.

[14] Gustavsen B, Semlyen A. Simulation of transmission line transients using vector fitting and modal decomposition. IEEE Trans Power Deliv 1998;13(2):605–14. http://dx.doi.org/10.1109/61.660941.

[15] Costa ECM, Kurokawa S, Pissolato J, Prado AJ. Efficient procedure to evaluate electromagnetic transients on three-phase transmission lines.. IET Gener Transm Distrib 2010;4:1069–81. http://dx.doi.org/10.1049/iet-gtd.2009.0660.

[16] Costa ECM, Kurokawa S, Pinto AJG, Kordi B, Pissolato. Simplified computational routine to correct modal decoupling in transmission lines and power systems modeling. IET Sci Meas Technol 2013;7:7–15. http://dx.doi.org/10.1049/iet-smt.2012.0057.

[17] Ametani A, Ohno T, Nagaoka N. Cable system transients: Theory, modeling and simulation. New York: Wiley-IEEE Press; 2015, p. 1–550.

[18] Chien CH, Bucknall RWG. Theoretical aspects of the harmonic performance of subsea ac transmission systems for offshore power generation schemes. IEEE Proc Gener Transm Distrib 2006;153(5):599–609. http://dx.doi.org/10.1049/ip-gtd:20060036.

[19] Silva RC, Kurokawa S, Costa ECM, Pissolato J. Development of a simplified transmission line model directly in the phase domain. In: 2012 IEEE power and energy society general meeting. 2012, p. 1–8. http://dx.doi.org/10.1109/PESGM.2012.6345078.

[20] Souza NV, Carvalho CG, Kurokawa S, Pissolato J. A distributed-parameters transmission line model developed directly in the phase domain. Electr Power Compon Syst 2013;41(11):1100–13. http://dx.doi.org/10.1080/15325008.2013.809823.

[21] Gómes P, Uribe FA. The numerical Laplace transform: An accurate technique for analyzing electromagnetic transients on power system devices.. Int J Electr Power Energy Syst 2009;31:116–23. http://dx.doi.org/10.1016/j.ijepes.2008.10.006.

[22] Gustavsen B. Relaxed vector fitting algorithm for rational approximation of frequency domain responses. In: IEEE workship on signal propagation on interconnects. 2006, p. 97–100. http://dx.doi.org/10.1109/SPI.2006.289202.

[23] Caballero PT, Costa ECM, Kurokawa S. Frequency dependent multiconductor line model based on the Bergeron method. Electr Power Syst Res 2015;127:314–22. http://dx.doi.org/10.1016/j.epsr.2015.05.019.

[24] Costa ECM, Kurokawa S, Pinto AJG, Kordi B, Pissolato J. Simplified computational routine to correct the modal decoupling in transmission lines and power systems modelling. IET Sci Meas Technol 2013;7(1):7–15. http://dx.doi.org/10.1049/iet-smt.2012.0057.